A first-principles study of CO oxidation by surface oxygen on Pt-incorporated perovskite catalyst ($CaPt_xTi_{1-x}O_3$)

Qiuju Zhang,[a] Baihai Li,[ab] Houyuan Wang,[a] Yange Suo[a] and Liang Chen*[a]

In the present work, we investigated the structural and catalytic properties of a prototype system Pt-doped $CaTiO_3$ by means of first principles calculations. We paid particular attention to the aggregation and penetration of Pt on different surfaces of $CaTiO_3$, and subsequent CO oxidation by surface oxygen atoms on Pt-doped $CaTiO_3$. Our calculations indicate that CO oxidation can potentially take place when Pt is doped on the first layer of $CaTiO_3$(001). The activation barriers are calculated to be 0.20–0.45 eV. The possibly induced O vacancy on the surface will produce a magnetic behavior by breaking the spin density symmetry due to one Pt–O bond cleavage. Our study is expected to provide an insight into the catalytic behavior of Pt ions in Pt-doped perovskite toward the oxidation of exhaust gas.

I Introduction

Oxide-supported precious-metal particles have attracted intense interest due to their wide applications in heterogeneous catalysis. However, the well-known strong metal-support interactions (SMSI) for group VIII (8–10) noble metals on oxide often drastically reduce their catalytic performance.[1] For example, noble-metal-promoted perovskites, potentially used as automobile exhaust catalysts, exhibit typical SMSI that leads to severe catalyst deactivation.[2] This deterioration is generally compensated by loading an excess of precious metal, which could result in overconsumption of limited noble metal resources.[3,4] Therefore, effectively maintaining or increasing the catalytic activity and controlling the consumption of precious metals are highly demanded. Recently, it was observed that the incorporation of precious metal into perovskite lattice is helpful to increase their catalytic ability. The presence of ionic Pd, Pt or Rh in a perovskite matrix, in most cases, is responsible for the high activity of noble-metal-promoted perovskites.[5,6] For example, $BaCeO_3$ was experimentally observed to incorporate Pd(II) into B sites to form $BaCe_{1-x}Pd_xO_{3-\delta}$, which maximized the catalytic activity for CO oxidation due to the presence of cationic Pd(II) in the perovskite host.[2] Similarly, the experimentally observed high-temperature activity of $LaPdCoO_3$ for lean NO_x reduction was also linked to the presence of ionic Pd in the $LaCoO_3$ matrix.[7]

Motivated by the high activity of Pd ions in $BaCe_{1-x}Pd_xO_{3-\delta}$, we attempted to investigate the structural and catalytic properties of prototype $CaPt_xTi_{1-x}O_3$ system by means of first principles calculations. Actually, the incorporation of noble metal into the B site of perovskite (ABO_3) lattice has been originally found for Pd-doped perovskites ($LaFeCoPdO_3$ and $LaFePdO_3$) due to the self-regeneration abilities of Pd, *i.e.*, Pd could be reversibly incorporated into the perovskite lattice and segregate out, as the exhaust gas is cycled between oxidizing and reducing conditions.[8,9] The perovskite exhibiting self-regeneration feature is named as "intelligent catalysis" (IC), which was afterward extended to Pt and Rh-doped $CaTiO_3$ systems.[6] By using X-ray and transmission electron microscope (TEM) techniques, Scott *et al.* observed that Rh or Pt in the doped $CaTiO_3$ could move in and out of the perovskite structure with the fluctuation of oxidation and reduction atmospheres.

In this work, the self-regeneration of single-atom Pt deposition on or penetration into CaO- and TiO_2-terminated $CaTiO_3$ system was initially studied to evaluate the possibility of the presence of Pt cation. After that, the possible enhancement of surface oxygen activity toward CO oxidation by the presence of Pt substitution was explored by performing climbing nudged elastic band (cNEB) calculations.[10–12] The produced oxidation product CO_2 was found to be desorbed from TiO_2-terminated surface and create an O vacancy, which will induce a spin splitting of Pt-5d electron below the Fermi level, to cause magnetism transformation. Thus, we expect that the magnetism transition from non-magnet of stoichiometric $CaTi_{1-x}Pt_xO_3$ to magnetic $CaTi_{1-x}Pt_xO_{3-\delta}$ can be applied to monitor such oxidation process in the experimental characterization.

II Computational methods

Spin polarized DFT calculations were performed using the Vienna *ab initio* simulation package (VASP).[13] The electron

[a]*Ningbo Institute of Materials Technology and Engineering, Chinese Academy of Sciences, Ningbo, Zhejiang 315201, P. R. China. E-mail: chenliang@nimte.ac.uk*

[b]*School of Energy Science and Engineering, University of Electronic Science & Technology of China, Chengdu 611731, P. R. China*

exchange and correlation were treated within the generalized gradient approximation (GGA)[14] using the PW91 functional.[15–17] The projector-augmented-wave (PAW) method of Blöchl[18] was used for the treatment of the core electrons. A soft potential was employed for oxygen (O_s, $2s^2 2p^4$, cutoff energy of 250 eV), while a plane wave cutoff of 350 eV was chosen in all calculations. Monkhorst Pack (MP) grid[19] of ($2 \times 2 \times 1$) were used for the (2×2) $CaTiO_3$ (001) surface. In order to avoid the dipole–dipole interactions between periodic slabs, we built the slab models consisting of 7 atomic layers with CaO or TiO_2 as the termination for both sides. A vacuum spacing of 14 Å was added in the perpendicular direction. All atoms were fully relaxed with the forces converged to less than 0.03 eV $Å^{-1}$. The Methfessel–Paxton technique[20] with a smearing width of $\sigma = 0.1$ eV was used to minimize the errors in the Hellmann–Feynman forces. The optimized lattice constants ($a = 5.394$ Å, $b = 5.512$ Å, $c = 7.685$ Å) are in good agreement with experimental results ($a = 5.381$ Å, $b = 5.442$ Å, $c = 7.641$ Å).

To ascertain whether Pt could penetrate into replace $CaTiO_3$ host to replace Ti ions, the configurations of $CaTi_{1-x}Pt_xO_3$ are generated by the cluster expansion (CE) formalism.[21–24] For the binary system, CE can be written as

$$E(\vec{\sigma}) = V_0 + \sum_i V_i \sigma_i + \sum_{i,j} V_{ij} \sigma_i \sigma_j + \sum_{i,j,k} V_{ijk} \sigma_i \sigma_j \sigma_k + \ldots \quad (1)$$

where V_i, V_{ij}, V_{ijk},…are the effective cluster interactions (ECIs), σ is a spin-like occupation variable (*e.g.*, $\sigma = 1$ if the B-site of $CaTiO_3$ perovskite matrix is occupied by Ti, and $\sigma = -1$ if the site is occupied by Pt). The coefficients are obtained by fitting eqn (1) to the first principles calculated energies of the selected subset from the configurations generated by CE. In principle, CE should take all the pairs, triplets, quadruples, *etc.* into account; however, in practice the cluster expansion can efficiently predict the energy of a system based on fewer coefficients. The optimal coefficient can be obtained according to the cross-validation (CV) score by using a genetic algorithm.[21,25–28]

III Results and discussions

A. Deposition and migration of Pt on $CaTiO_3$(001) surfaces

First of all, we attempt to investigate the binding of Pt atom on the two commonly observed CaO- and TiO_2-terminated surfaces. Similar to the previously studied Pd-doped $LaFeO_3$ system,[29,30] the one-fold O_I site at the CaO-terminated surface and the four-fold O_H site at TiO_2-terminated surface are found to be the most favorable binding positions for Pt (see Fig. 1). In the calculations, Pt on other trial sites will converge to these two sites upon structural optimizations. As shown in Fig. 1a and b, Pt binds to the outmost O_I on CaO-terminated surface with the bond length of 1.93 Å and tilting angle ($\angle$PtOO) of about 55°, yielding a binding energy (E_b) of 2.93 eV. In the case of TiO_2-terminated surface, Pt is preferentially located on the O_H hollow site, yielding a slightly higher E_b of 3.10 eV. Upon the deposition of Pt, the four coordinated O_H atoms would be dragged out of surface by around 0.30 Å to form four Pt–O_H bonds with bond lengths in the range of 2.01–2.05 Å.

Interestingly, the charge distribution analysis displays some distinctive features for the charge transfer between the two surfaces. Specifically, Pt gains 0.55 electron from the CaO-terminated surface, whereas donates 0.63 electron to the TiO_2-terminated surface. This can be understandable since the CaO-terminated and TiO_2-terminated surfaces are electron-rich and electron-poor, respectively. According to the Bader charge analysis, the net charges on the CaO-terminated and TiO_2-terminated surfaces are calculated to be $-0.30|e|$ and $+0.73|e|$, respectively. In the Bader analysis, each atom is divided based on the zero flux surfaces those are 2-D surfaces on which the charge density is a minimum perpendicular to surface. To present further evidence of electron transfer between Pt and $CaTiO_3$ surfaces, we also calculated the electron density difference between the adstructures and separate components with each atom frozen at their optimized positions. It is clearly shown in Fig. 1c and c′ that Pt–O bonds are formed on both

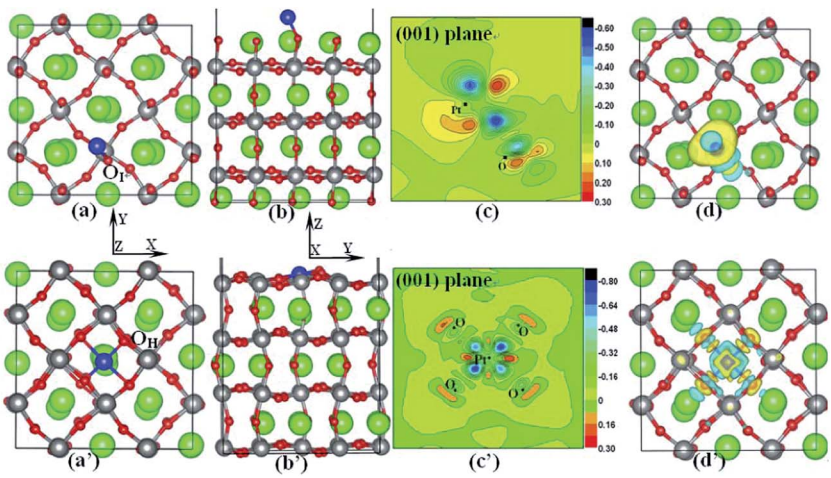

Fig. 1 Single Pt atom adsorption on CaO and TiO_2-terminated surface. (a–d) provide the topview and sideview of single Pt atom deposition on CaO-terminated surface, and its 2D and 3D electron energy difference; (a′–d′) shows the corresponding parts of single Pt atom deposition on TiO_2-terminated surface. The green, grey, red and blue balls represent Ca, Ti, O and Pt atoms, respectively.

surfaces after electron transfer. The 3D yellow spherical shapes (denoting electron-rich area) in Fig. 1d indicates that Pt serves as electron acceptor on the CaO-terminated surface. In contrast, the light-blue shapes (denoting electron-poor area) of Pt on TiO_2-termiated surface shows electron donating behavior.

Since metal aggregation is usually the major concern for the supported catalysts, we next studied the aggregation tendency of Pt on the two surfaces. As only one favorable binding site is identified for each surface, we evaluated the migration of Pt between two nearest O_I sites on CaO-termination and two nearest O_H sites on TiO_2-termination. The transition state is identified by performing cNEB calculations along the prescribed pathways, as shown in Fig. 2. The calculated energy barriers for Pt migration on CaO and TiO_2-terminations are 1.18 and 1.71 eV, respectively. Such high barriers indicate that the migration of Pt is difficult to take place between two nearest O_I or O_H sites. An intermediate state of O–Pt–O bonding is found on the migration pathway of Pt/TiO_2-term, which is also obtained by the initial optimization as a meta-stable state.

B. The incorporation of Pt into $CaTiO_3$ lattice

We next estimated the possibility of Pt penetration into the B site of $CaTiO_3$ lattice in terms of thermodynamics. Here, we calculated the binding energy ($E_b = E_{total} - E_{vacancy\text{-}Ti} - E_{Pt}$) for Pt with the Ti vacancy at different layers, as shown in Fig. 3a. E_b is calculated to be 9.52 eV for the substitution of the 1st-layer Ti (denoted as "Pt_{Ti}^{1st}" hereafter), which is increased to 9.81 eV when Pt replaces the second (denoted as "Pt_{Ti}^{2nd}" hereafter) and third layer Ti (denoted as "Pt_{Ti}^{3rd}" hereafter). The larger E_b of Pt_{Ti}^{2nd} and Pt_{Ti}^{3rd} means Pt tend to penetrate deep into the $CaTiO_3$ lattice, which is consistent with the experimental observation that Pt could dissolve into the $CaTiO_3$ lattice under oxidizing atmosphere.[6] Actually, it is reasonable that E_b for Pt_{Ti}^{2nd} is greater than that of Pt_{Ti}^{1st} because Pt forms five Pt–O bonds in a square-pyramid coordination with the bond length of 1.97–2.03 Å in Pt_{Ti}^{1st} while it forms six Pt–O bonds in octahedron coordination with the bond length of 2.02–2.03 Å in Pt_{Ti}^{2nd}.

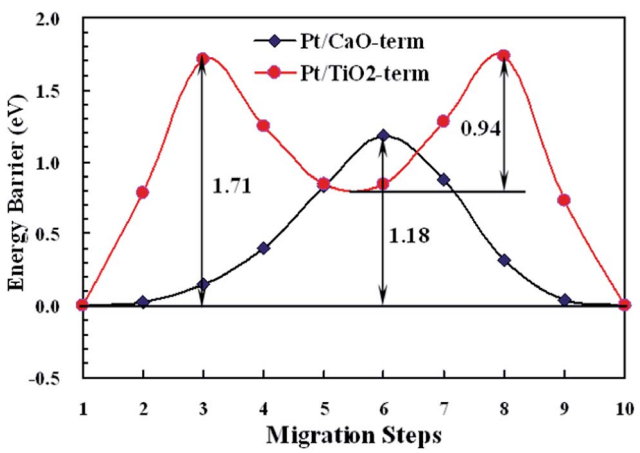

Fig. 2 The migration barriers of single Pt atom between the nearest O_I and O_H sites on CaO- and TiO_2-terminated surface, respectively.

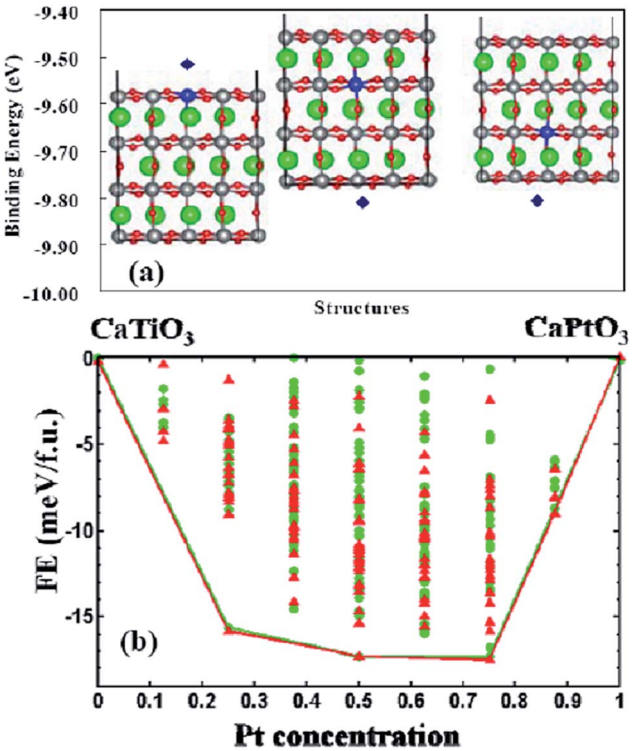

Fig. 3 (a) The structures of Pt penetration into different layer Ti to form Pt–$CaTiO_3$; (b) convex hulls of the formation energies per formula unit (FE/f.u.) of Pt doped $CaTiO_3$ structures based on first principles calculation and cluster expansion. Data obtained by VASP and CE are colored red and green, respectively.

To further ascertain whether Pt could replace Ti ions of $CaTiO_3$ and the corresponding stability, we calculated the formation energies of $CaTi_{1-x}Pt_xO_3$ by DFT methods according to $E_f = E_{CTPO} - xE_{CPO} - (1-x)E_{CTO}$, where E_{CTPO}, E_{CPO} and E_{CTO} are the total energies of $CaTi_{1-x}Pt_xO_3$, $CaPtO_3$ and $CaTiO_3$, respectively, x is the Pt doping concentration. The formation energies obtained by DFT calculations were verified by the CE prediction and a good correlation between them was obtained. The weighted CV score is 3.3 meV/f.u. with a root mean square (rms) error of 1.4 meV/f.u. in the CE validation process. The comparison between the DFT calculated (red points) and CE predicted (green points) formation energies are shown in Fig. 3b, respectively. The convex hull obtained by CE (green line) is well-converged and accurately reproduces that of the DFT ground states (red line). The negative formation energies of $CaTi_{1-x}Pt_xO_3$ indicate the feasibility of Pt occupying the Ti sites. However, the energy differences between the ground states and other structures are only several meV/f.u., implying that the $CaTi_{1-x}Pt_xO_3$ structures would probably become a disordered solid solution above moderate temperatures.

C. CO oxidation by surface oxygen

Since the lattice oxygen has been verified to not oxidize CO in bare TiO_2(110) surface,[31] it is natural to ask whether such oxidation process will occur in the presence of ionic Pt in TiO_2-terminated surface. To explore the possible catalytic

enhancement by Pt incorporation into the perovskite host, we focus on the CO oxidation by surface oxygen in Pt_{Ti}^{1st} and Pt_{Ti}^{2nd} TiO_2-termination. Inspired by the recent observation of single Pt atom loaded on FeO_x nanocrystallite support or graphene to form Pt_1/FeO_x or Pt/graphene, respectively,[32,33] we built a model of single Pt atom deposited on the surface or occupying the B site of $CaTiO_3$ to form $CaPt_xTi_{1-x}O_3$ to minimize the computational cost and examine its catalytic behavior. We found that CO can be favorably adsorbed on the Pt site to form linear chemisorption state *via* the C or O ends in the Pt_{Ti}^{1st} structure (see Fig. 4a). Apparently, the C end can interact with the ionic Pt more strongly, with an adsorption energy ($E_{ads.} = E_{CTPO} + E_{CO} - E_{CO\text{-}CTPO}$) of 1.59 eV and shorter Pt–C distance of 1.86 Å. In contrast, the O end can interact with Pt with an E_{ads} of 0.16 eV and O–Pt distance of 2.13 Å, respectively. For comparison, we also investigated the CO adsorption on Pt deposited onto stoichiometric TiO_2-terminated surface instead of replacing the Ti ion. Upon optimization, the CO molecule initially placed 2.1 Å above the surface Pt atom, would be pushed away in spite of C and O ends, as shown in Fig. 4c, which illustrates that the Pt atom deposited on TiO_2 surface completely loses its reactivity toward CO molecule. Actually, this is reasonable because the four lobes of Pt-5d orbital become inaccessible after the formation of four Pt–O coordination on TiO_2 surface, similar to our previous study of H_2 chemisorption on Pt/MoO_3.[34]

For the Pt_{Ti}^{2nd} structure, the Pt atom is embraced underneath and not available for interacting with CO. Nevertheless, CO can be still linearly chemisorbed on the Ti site *via* the C end. The distance between C end and Ti is calculated to be 2.34 Å, as depicted in Fig. 4b. Although the corresponding $E_{ads} = 0.10$ eV is significantly weaker than that of Pt_{Ti}^{1st}, the reactive activity of Ti is actually enhanced by loading Pt since CO can be hardly adsorbed on the TiO_2-terminated surface of the pure $CaTiO_3$.

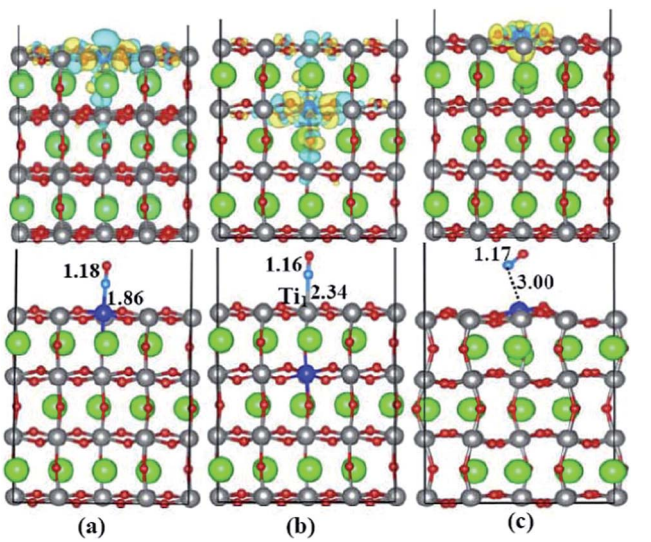

Fig. 4 The bottom presents adstructures of CO adsorption on Pt_{Ti}^{1st}, Pt_{Ti}^{2nd} and Pt deposition on TiO_2-terminated surface through C end. The top is the corresponding calculated 3D electron density difference of Pt-doped $CaTiO_3$(001) with TiO_2-termination.

The similar phenomenon can be found in the case of CO activation on $BaCe_{0.90}Pd_{0.10}O_{3-\delta}$ and undoped $BaCeO_3$, in which the higher activity associated with $BaCe_{0.90}Pd_{0.10}O_{3-\delta}$ is reflected by lower light-off temperature ($T_{50} = 83$ °C), compared with $T_{50} = 225$ °C for the undoped $BaCeO_3$.[2]

To ascertain the intrinsic mechanism of the improved surface activity, the 3D electron density difference is plotted for these Pt-doped and undoped structures in Fig. 4. For the Pt_{Ti}^{1st} structure, it is clearly shown that the five-coordinated Pt atom accumulates some electrons (blue contour) along the surface normal (Fig. 4a) due to the absence of one Pt–O bond. The remained electron on the unsaturated Pt atom is responsible for the high reactivity toward CO adsorption. After further incorporating Pt into the second TiO_2 layer, the surface Ti atom obtains some electrons through the Pt–O–Ti bond (Fig. 4b), which enhances the reactivity of Ti compared to other surface Ti ions. In contrast, no electron accumulation along the surface normal can be observed nearby the Pt atom deposited on the stoichiometric TiO_2-terminated surface. As shown in Fig. 4c, only yellow contour of denoting electron deficient in this direction was remained due to the tetra- Pt–O bonds formation.

As discussed above, TiO_2-terminated surface exhibits electron-poor feature evidenced by Bader charge analysis, which results in the ability of attracting electron in the surface. We next evaluate the possibility of CO oxidation on surface oxygen following the two chemisorption states. For the adstructure (Pt–CO) through C end, the C atom is able to further bind with the neighbored O_1 and drags it out of the surface by about 0.90 Å to form a bent CO_2 structure, yielding a bent angle $\angle OCO = 140°$ and E_{ads} of 2.08 eV. We term this state as CO_2-bending. From the kinetic point of view, the adsorbed CO needs to overcome a barrier of 0.45 eV at the transition state TS_I to bind with O_1 atom, as depicted in path I of Fig. 5. The bond length of two newly formed C–O bonds is slightly elongated from 1.18 Å to 1.21 Å due to the slight disturbance of C≡O triplet bond.

The oxidation process is also found to potentially take place for CO adsorbed through the O end (Pt–OC). Since adsorption on Pt^{1st} *via* the O end results in smaller energy, the upstanding C atom will continue to increase its E_{ads} to 0.34 eV by binding with O_1 atom with a bent angle of $\angle OCO = 106°$. In contrast to the η^2(CO) structure, this bent CO_2-TM state should be ascribed to η^2(COO) state because the two O atoms are directly bonded with Pt. The newly formed C–O_1 bond of 1.38 Å will also drag the O_1 atom out of TiO_2 surface by about 0.8 Å. The calculated activation barrier of 0.20 eV toward CO oxidation is even smaller than that of the commonly used Au–Cu catalyst (activation barrier = 0.60 eV).[35] In the TS_{II}^1, the original C=O bond length is elongated to 1.20 Å and C–O_1 distance is decreased to 2.34 Å. More interestingly, such oxidation state η^2(COO) is actually an intermediate and would converge to the most stable CO_2-bending state η^2(CO) eventually. The similar conversion has also been found in the previous CO_2-TM state, in which COO binding is not a stable state.[36,37] In the TS_{II}^2 (Fig. 5), the distance of C–Pt is shortened to 2.67 Å, while the original Pt–O bond is increased to 2.48 Å, yielding an activation barrier of 0.26 eV.

Whether the product (free CO_2 molecule) could be desorbed from such η^2(CO)–Pt complex is another key issue for the

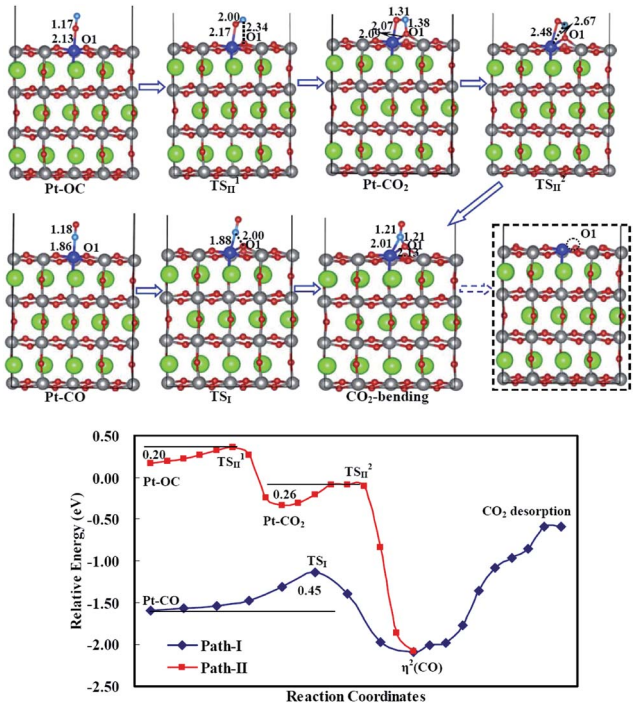

Fig. 5 The CO oxidizing process by the surface O1 atom on TiO_2-terminated surface of Pt-substitution the first layer Ti. Path I and II refer to the two reaction pathways through C and O ends. The corresponding structures and the bond length are also presented.

catalytic activity. As depicted in Fig. 5, the CO_2 desorption will increase its thermal energy by about 1.45 eV compared to η^2(CO)–Pt complex, yielding an activation barrier of 1.45 eV in this process. Such a high activation barrier is generally difficult to conquer, however, the exothermic energy (about 2.1 eV) of forming η^2(CO) in path II possibly accumulate enough energy to enable the desorption of CO_2. It is noteworthy here that the high-barrier reaction pathway II only plays a minor role in the CO oxidation process, compared to the low-barrier reaction pathway I. Furthermore, an O-vacancy on TiO_2-terminated surface will be induced by CO_2 desorption, as shown in the dashed box in Fig. 5. Although no obvious deformation can be discerned except for the slightly elongated bond length of Pt–O bond opposite to Pt–$O_{vacancy}$, the electron feature near Fermi level is significantly different from the stoichiometric Pt–$CaTiO_3$. Fig. 6a clearly shows that the whole electronic bands are downshifted by approximately 0.5 eV in TiO_2-terminated surface with an O-vacancy. An obvious spin splitting at valence band maximum (VBM) is discerned by destroying the symmetric electronic bands of stoichiometric $CaTi_{1-x}Pt_xO_3$, although the band gap is nearly unchanged. Such electron variation will probably induce magnetism transformation from non-magnet of stoichiometric $CaTi_{1-x}Pt_xO_3$ to magnetic $CaTi_{1-x}Pt_xO_{3-\delta}$, which is further confirmed by the calculated total magnetic moment of 1.90 μ_B in $CaTi_{1-x}Pt_xO_{3-\delta}$. Projected density of states (PDOS) indicates that the split electronic band in VBM is mainly ascribed to the splitting of Pt-5d bands, as shown in Fig. 6b, which is consistent with the calculated local magnetic moment of 1.10 μ_B on Pt. Compared to the original

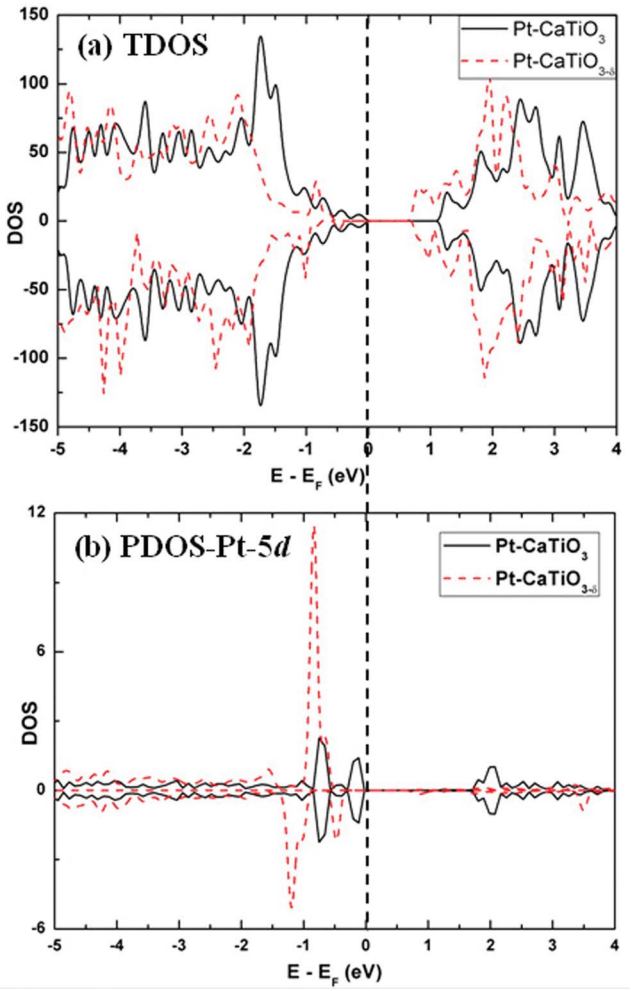

Fig. 6 Comparison of the total density of states (TDOS) (a) for O-vacant (Pt–$CaTiO_{3-x}$) and Pt-$CaTiO_3$ and the projected local density of states (PDOS) of Pt-5d band (b) to illustrate their electromagnetic behavior near Fermi level.

smaller peak, Pt-5d band becomes more narrow and stronger. Such emergence of magnetism is contributed by the broken symmetric square-pyramid structure of five-coordination of Pt, and is expected to be helpful to monitor the surface oxygen function states in the CO oxidation process.

IV Conclusion

Based on the DFT and CE calculations, both the increased binding energy with Pt penetration and the negative formation energy of $CaTi_{1-x}Pt_xO_3$ indicate the feasibility of replacing Ti sites in $CaTiO_3$ by Pt, which is consistent with the experimentally observed self-regeneration of Pt particles on $CaTiO_3$. The penetrated Pt ion could enhance the surface activity of $CaTiO_3$ to form two adsorption states through the C and O ends. Further, we show that following oxidation by the surface O atom could readily take place to yield more stable η^2(CO)–Pt complex, due to the low activation barrier of 0.45 eV and 0.20 eV in the pathways I and II. From the whole reaction energy profile, CO

oxidation path I is dominate process owning to the lower thermal energy along the oxidation process. However, the minor oxidation path II is possible to induce CO_2 desorption and hence cause a magnetic transition (*i.e.*, from non-magnetic $CaTiO_3$ to magnetic $CaTiO_{3-\delta}$). Our study is expected to provide an insight of catalytic behavior of Pt ion in Pt-doped perovskite toward exhaust gas oxidation. The magnetism transition could possibly used as a measurement to monitor the oxidation process.

Acknowledgements

We gratefully acknowledge the financial support by the national key basic research program of China (Grant nos 2013CB934800 and 2012CB722700), national science foundation of China (Grant no. 21003144, 11274323), innovative research project of Ningbo municipal government (Grant no. 2011B82005), Ningbo NSF (2012A610117 and 2012A610099), and China postdoctoral science foundation funded project (2013M530292).

References

1 S. J. Tauster, *Acc. Chem. Res.*, 1987, **20**, 389.
2 U. G. Singh, J. Li, J. W. Bennett, A. M. Rappe, R. Seshadri and S. L. Scott, *J. Catal.*, 2007, **249**, 349.
3 Z. X. Tian, K. Inagaki and Y. Morikawa, *Curr. Appl. Phys.*, 2012, **12**, S105.
4 B. Li, O. K. Ezekoye, Q. Zhang, L. Chen, P. Cui, G. Graham and X. Pan, *Phys. Rev. B.*, 2010, **82**, 125422.
5 H. Tanaka, M. Taniguchi, N. Kajita, M. Uenishi, I. Tan, N. Sato, K. Narita and M. Kimura, *Top. Catal.*, 2004, **30–1**, 389.
6 M. Taniguchi, H. Tanaka, M. Uenishi, I. Tan, Y. Nishihata, J. I. Mizuki, H. Suzuki, K. Narita, A. Hirai and M. Kimura, *Top. Catal.*, 2007, **42–43**, 367.
7 I. Twagirashema, M. Engelmann-Pirez, M. Frere, L. Burylo, L. Gengembre, C. Dujardin and P. Granger, *Catal. Today*, 2007, **119**, 100.
8 Y. Nishihata, J. Mizuki, T. Akao, H. Tanaka, M. Uenishi, M. Kimura, T. Okamoto and N. Hamada, *Nature*, 2002, **418**, 164.
9 H. Tanaka, M. Taniguchi, M. Uenishi, N. Kajita, I. Tan, Y. Nishihata, J. I. Mizuki, K. Narita, M. Kimura and K. Kaneko, *Angew. Chem., Int. Ed.*, 2006, **45**, 5998.
10 H. Jonsson, *Annu. Rev. Phys. Chem.*, 2000, **51**, 623.
11 G. Henkelman, B. P. Uberuaga and H. Jonsson, *J. Chem. Phys.*, 2000, **113**, 9901.
12 G. Henkelman and H. Jonsson, *J. Chem. Phys.*, 2000, **113**, 9978.
13 G. Kresse and J. Hafner, *Phys. Rev. B.*, 1993, **48**, 13115.
14 J. P. Perdew, J. A. Chevary, S. H. Vosko, K. A. Jackson, M. R. Pederson, D. J. Singh and C. Fiolhais, *Phys. Rev. B.*, 1992, **46**, 6671.
15 J. P. Perdew, J. A. Chevary, S. H. Vosko, K. A. Jackson, M. R. Pederson, D. J. Singh and C. Fiolhais, *Phys. Rev. B.*, 1993, **48**, 4978.
16 J. P. Perdew, K. Burke and M. Ernzerhof, *Phys. Rev. Lett.*, 1996, **77**, 3865.
17 J. P. Perdew, K. Burke and M. Ernzerhof, *Phys. Rev. Lett.*, 1997, **78**, 1396.
18 P. E. Blöchl, *Phys. Rev. B.*, 1994, **50**, 17953.
19 H. J. Monkhorst and J. D. Pack, *Phys. Rev. B.*, 1976, **13**, 5188.
20 M. Methfessel and A. T. Paxton, *Phys. Rev. B.*, 1989, **40**, 3616.
21 A. van de Walle and G. Ceder, *J. Phase Equilib.*, 2002, **23**, 348.
22 A. Van der Ven, J. C. Thomas, Q. C. Xu and J. Bhattacharya, *Math. Comput. Simul.*, 2010, **80**, 1393.
23 J. M. Sanchez, F. Ducastelle and D. Gratias, *Phys. A*, 1984, **128**, 334.
24 A. Van der Ven, H. C. Yu, G. Ceder and K. Thornton, *Prog. Mater. Sci.*, 2010, **55**, 61.
25 G. L. W. Hart, V. Blum, M. J. Walorski and A. Zunger, *Nat. Mater.*, 2005, **4**, 391.
26 Q. Xu and A. Van der Ven, *Phys. Rev. B.*, 2007, **76**, 064207.
27 A. Van der Ven, J. C. Thomas, Q. C. Xu and J. Bhattacharya, *Math. Comput. Simul.*, 2010, **80**, 1393.
28 J. M. Sanchez, F. Ducastelle and D. Gratias, *Phys. A*, 1984, **128**, 334.
29 A. Van der Ven, H. C. Yu, G. Ceder and K. Thornton, *Prog. Mater. Sci.*, 2010, **55**, 61.
30 B. Li, M. B. Katz, Q. Zhang, L. Chen, G. W. Graham and X. Pan, *J. Chem. Phys.*, 2013, **138**, 144705.
31 X. Y. Wu, A. Selloni and S. K. Nayak, *J. Chem. Phys.*, 2004, **120**, 4512.
32 B. Qiao, A. Wang, X. Yang, L. F. Allard, Z. Jiang, Y. Cui, J. Liu, J. Li and T. Zhang, *Nat. Chem.*, 2011, **3**, 634.
33 S. Sun, G. Zhang, N. Gauquelin, N. Chen, J. Zhou, S. Yang, W. Chen, X. Meng, D. Geng, M. N. Banis, R. Li, S. Ye, S. Knights, G. A. Botton, T.-K. Sham and X. Sun, *Sci. Rep.*, 2013, **3**, 1775.
34 B. Li, W.-L. Yim, Q. Zhang and L. Chen, *J. Phys. Chem. C*, 2010, **114**, 3052.
35 A. Hussain, *J. Phys. Chem. C*, 2013, **117**, 5084.
36 Q. Zhang, L. Cao, B. Li and L. Chen, *Chem. Sci.*, 2012, **3**, 2708.
37 D. H. Gibson, *Chem. Rev.*, 1996, **96**, 2063.